# Solidification of Gold Nanoparticles in Carbon Nanotubes

S. Arcidiacono,[1] J. H. Walther,[2,3] D. Poulikakos,[1,*] D. Passerone,[3] and P. Koumoutsakos[2,3]
[1]*Laboratory of Thermodynamics in Emerging Technologies, ETH, Zurich, Switzerland*
[2]*Institute of Computational Science, ETH, Zurich, Switzerland*
[3]*Computational Laboratory, ETH, Zurich, Switzerland*
(Received 22 October 2004; published 18 March 2005)

The structure and the solidification of gold nanoparticles in a carbon nanotube are investigated using molecular dynamics simulations. The simulations indicate that the predicted solidification temperature of the enclosed particle is lower than its bulk counterpart, but higher than that observed for clusters placed in vacuum. A comparison with a phenomenological model indicates that, in the considered range of tube radii ($R_{\mathrm{CNT}}$) of $0.5 < R_{\mathrm{CNT}} < 1.6$ nm, the solidification temperature depends mainly on the length of the particle with a minor dependence on $R_{\mathrm{CNT}}$.

DOI: 10.1103/PhysRevLett.94.105502 PACS numbers: 61.46.+W, 64.70.Dv, 65.80.+n, 71.15.Pd

The presence of enclosed nanoparticles in carbon nanotubes (CNTs) is known to alter the CNT properties, making feasible several promising applications (catalysis, semiconductor devices, contrast agents in magnetoresonance imaging, etc.). A number of works has addressed the practical process of the filling of CNTs with different metals (see [1] and references therein). The structure and melting of nanowires of some metals (Cs, Cu, *K*) inside zigzag (*n, n*) carbon nanotubes at different values of *n* were studied using MD simulations [1–3]. A cylindrical shell structure was found for all the wires with smaller CNT radii, while at larger radii the predicted structure consisted of an fcc core for the Cu particles [1] and a bcc core for the *K* particles [3]. In the aforementioned works nanowires inside CNTs showed a higher melting temperature compared to isolated nanowires indicating that the CNT wall increases the stability of the encapsulated nanowires. The shell structure of isolated nanowires was also predicted computationally [4] and observed experimentally [5]. A numerical study of Wang *et al.* [6] on gold nanowires with diameters ($D$) up to 3 nm predicted that the wire structure is helical for $D < 0.6$ nm, multiwalled cylindrical for $1.0 < D < 2.2$ nm, and an fcc for $D > 2.2$ nm. The stability of finite length gold nanowires [7] and the melting of infinite gold nanowires [8] were studied in the past with molecular dynamics (MD) simulations, and a melting temperature ($T_M$) of $1000 \pm 100$ K was found [8]. These values for $T_M$ are intermediate between the bulk case and the corresponding finite gold nanowires [7]. Guo *et al.* [9] studied the structural transition of copper nanowires in single walled carbon nanotubes and found that the combined effect of pressure and the cylindrical shape of CNT dominates the structural transition of the particle. Monte Carlo simulations and experiments on the melting of nitrobenzene and carbon tetrachloride within CNTs [10] showed no formation of common three-dimensional crystalline structures, but concentric layered structures that solidify into quasi-two-dimensional hexagonal crystals. The melting was found to start in the inner layers. Recently, Liu *et al.* [11] conducted experiments on gallium encapsulated in CNTs. $T_M$ was found to be of the same order or higher than the bulk one depending on the crystalline phase. No influence of the CNT radius ($R_{\mathrm{CNT}}$) was found on $T_M$ in the range $100\ \mathrm{nm} < R_{\mathrm{CNT}} < 200$ nm.

In spite of these previous studies, a convincing theoretical interpretation of the size effects affecting the thermodynamical stability of these systems, as well as a model for a phenomenological description of the carbon-metal interaction are still missing. An *ab initio* approach appears prohibitive at this stage for studying extended systems and the size dependence of their properties.

In this work we use classical MD simulations for studying in detail the solidification temperature ($T_S$) and the structural properties of gold nanoparticles within CNTs of three different chirality vectors: $(n, m) = (20, 0)$, $(30, 0)$, and $(40, 0)$. We distinguish among the different cases by specifying the number of gold atoms $N_{\mathrm{Au}}$ and the chirality index $n$ of the CNT. We investigate particles ranging from $N_{\mathrm{Au}} = 123$ to $N_{\mathrm{Au}} = 4983$. We find a particular dependence of $T_S$ on the geometrical shape, and propose a simple phenomenological model that describes the results of our simulations. The system is made of an infinitely long CNT simulated in a box of length 21.72 nm (replicated using periodic boundary conditions along the axis) and a cluster of gold inside the tube. The interactions are modeled by the glue potential [12] for the gold-gold interaction, the force field introduced in [13] for the carbon-carbon interaction, while the gold-CNT interaction is modeled with a Lennard-Jones (LJ) potential using the parameters given in [14] ($\varepsilon_{\mathrm{C\text{-}Au}} = 0.01273$ eV, $\sigma_{\mathrm{C\text{-}Au}} = 2.9943$ Å). The assumption of using a graphite-gold interaction to mimic the gold-CNT system does not take into account curvature effects. However, a number of studies have used interaction potentials pertaining to graphitic surfaces for describing interactions with CNTs [1–3,13,15]. Moreover, we have performed some validation studies with different LJ inter-

 

action parameters as suggested in [16] ($\varepsilon_{\text{C-Au}} = 0.022$ eV, $\sigma_{\text{C-Au}} = 2.74$ Å). The observed change in the $T_S$ compared to the simulations using the parameters reported in [14] [ca. 25 K difference for the case ($N_{\text{Au}} = 1316$, $n = 30$)] is within the uncertainty on the estimated $T_S$. Concerning the potential for gold, we are aware that the empirical ''glue'' potential has not been validated in the case of wires of nearly atomic thickness, and we therefore do not extend our analysis to such systems [4]. For all simulations, we use the MD package FASTTUBE [13], and we sample the canonical ensemble using a Berendsen thermostat [17]. The gold particle is inserted into the CNT and melted by bringing it to a temperature above the bulk $T_M$ (1400 K). The system is then successively cooled to different target temperatures using a cooling rate of 1 K/ps. Once a selected temperature is reached, the system is equilibrated until no significant oscillation of the average potential energy is observed; averages are collected for 1 ns.

The atomic positions for the case ($N_{\text{Au}} = 775$, $n = 30$) for the two different phases are presented in Fig. 1(a) (left side represents a solid phase, while right side represents a molten particle). The particle is composed of a cylindrical core of length $L$ and radius $R$ (Fig. 1) with two spherical end caps of height $h = R_c(1 - \sin\vartheta)$, where $\vartheta$ is the contact angle and $R_C = [-R/(\cos\vartheta)]$ the radius of curvature of the caps. A view along the axis of the CNT for the system ($N_{\text{Au}} = 775$, $n = 30$) at four different temperatures is shown in Fig. 1(b). A cylindrical layered structure, similar to that observed in nanowires, is present for all the cases. In Fig. 2(a), the radial density profiles for the same particle at different temperatures are shown. As expected, the peaks are higher at lower temperatures denoting a stronger layering. All peaks, especially the outermost ones, are shifted toward the center of the tube as the temperature increases. However, as shown in Fig. 2(a), the layered structure, induced by the CNT walls, is maintained at all temperatures, i.e., also in the molten state. A slightly different behavior of the radial density profile can be observed in particles enclosed in CNTs with $n = 40$ [Fig. 2(b)]. While peaks in the radial density distribution are also present both in the liquid and in the solid phases, the radial position of the innermost layers in the liquid phase is shifted outwards, compared to the corresponding peaks of the solid phase. Moreover, unlike in the case of $n = 30$, the magnitude of the peaks in the liquid phase decreases exponentially with the distance from the CNT walls. All these observations indicate a strong wall-induced layering. We note that gold exhibits layering also in the presence of a *free* molten surface [18].

To quantify this effect, we evaluated for each layer the two-dimensional orientational order parameter $Q_6$ [19]. For a perfect 2D triangular structure $Q_6 = 1$ and for an isotropic structure $Q_6 = 0$. $Q_6$ for the case ($N_{\text{Au}} = 1319$, $n = 30$) is plotted in Fig. 3 for all the studied temperatures. A 2D triangular structure with defects is present at lower temperatures, denoting the presence of a solid phase. The order is abruptly lost at the transition temperature of 1212 K. Some structure persists at the outermost layer as the temperature is further increased. This is in agreement with Ref. [10] and indicates that the presence of the CNT stabilizes the particle structure while melting starts at the center of the particle. On the contrary, Bilalbegović [8] found that in infinite isolated gold nanowires the melting occurs simultaneously in all shells. Similar results are obtained for the CNT with $n = 40$.

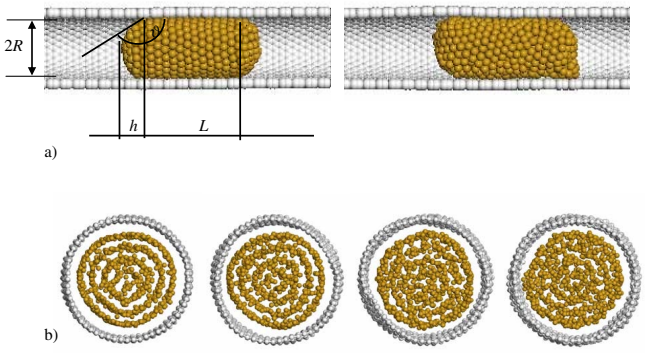


FIG. 1 (color online). (a) Time averaged atomic configuration of the Au nanoparticle and section of the carbon nanotube for the cases ($N_{\text{Au}} = 775$, $n = 30$) at 800 K (solid, left side) and 1400 K (liquid, right side). $L$ denotes the length of the cylindrical core, $R$ the radius, $\vartheta$ the contact angle, and $h$ the height of the cap. (b) Instantaneous view along the axis of the CNT for the system of ($N_{\text{Au}} = 775$, $n = 30$) at four different temperatures (400, 800, 1200, and 1400 K). The first two correspond to the solid phase, while the last two correspond to a liquid layered phase. The representation of the atomic radius is decreased with respect to (a) to distinguish the different layers.

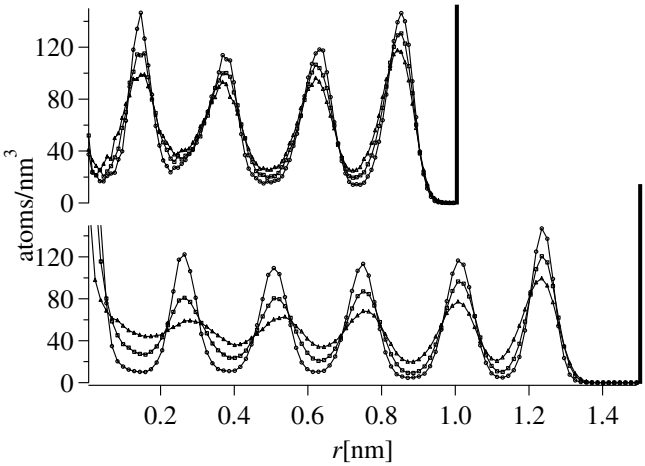


FIG. 2. Radial density profiles for the case at different temperatures. Circles, $T = 1100$ K; squares, $T = 1200$ K; triangles, $T = 1400$ K. (a) The case ($N_{\text{Au}} = 775$, $n = 30$), with $T_S = 1150$ K, and (b) the case ($N_{\text{Au}} = 4983$, $n = 40$), with $T_S = 1215$ K.

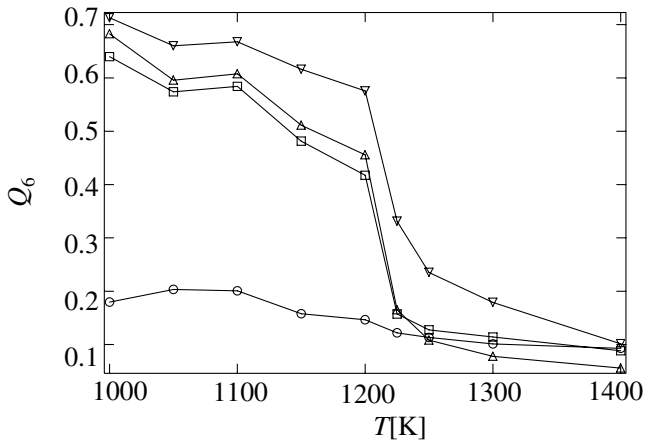


FIG. 3. Two-dimensional orientation order parameter $Q_6$ at different temperatures: Case ($N_{Au} = 1316$, $n = 30$). Circles: first layer (innermost); squares: second layer; up triangles: third layer; down triangles: fourth layer (outermost).

These results agree with the $T_s$ inferred from the potential energy as a function of temperature $T$ (not shown for brevity). The obtained $T_s$ is lower than its bulk counterpart $T_0$ at 1336 K and decreases with the number of gold atoms as reported in previous numerical and experimental works [20,21]. However, $T_s$ is higher compared to isolated clusters of the same mass in vacuum (Fig. 4, inset). The presence of the nanotube induces a partial recovery of the solidification temperature. It appears that two competing driving forces play a role: the finite size of the nanoparticle favoring disordering, and the solid wall of the CNT, inducing ordering and layering.

An understanding of the solidification behavior of a nanoparticle inside a CNT can be achieved by performing a free energy balance on the particle. The Gibbs free energy for the solid and the liquid phases can be written for the present geometrical configuration:

$$G_i = N\mu_i + 2\pi RL\gamma_{\text{C-}i} + 2A_c\gamma_i, \quad (1)$$

where $N$ is the number of atoms, $\mu_i$ the chemical potential of the phase $i$ ($s$, solid, or $l$, liquid), $A_c = 2\pi hr$ the approximate area of one spherical cap, $\gamma_{\text{C-}i}$ the surface tension between the CNT and the phase $i$, and $\gamma_i$ the surface tension of the phase $i$. The Gibbs-Duhem relationship near the solidification point and for an incompressible particle yields

$$N(\mu_s - \mu_l) = V\rho_s H(T - T_0)/T_0 + V(p_s - p_l), \quad (2)$$

where $V$ is the volume of the particle, $H$ the bulk latent heat of fusion, and $p_s$ and $p_l$ the pressures of the solid and liquid phases. Equating the Gibbs free energies of the two phases and accounting for (2) we obtain

$$(T_s - T_0)/T_0 = -\frac{2\pi RL\Delta\gamma_{\text{C-Au}}}{V\rho_s H} - \frac{2A_c\Delta\gamma_{\text{Au}}}{V\rho_s H} - \frac{p_s - p_l}{\rho_s H}, \quad (3)$$

where $\Delta\gamma_{\text{Au}} = \gamma_s - \gamma_l$ and $\Delta\gamma_{\text{C-Au}} = \gamma_{\text{C-}s} - \gamma_{\text{C-}l}$. The exact numerical value of $\Delta\gamma_{\text{C-Au}}$ is not known (to the best of our knowledge); hence, the first term of the right-hand side of (3) (specific for this confined geometry) cannot be directly evaluated.

All three terms in the right-hand side (rhs) of (3) contribute to decreasing $T_s$ with respect to the bulk value. For long particles, i.e., when the total volume $V$ is practically equal to the volume of the cylindrical core, $V_c = \pi LR^2$, the first term (including $\Delta\gamma_{\text{C-Au}}$) is inversely proportional to the radius of particle $R$. The second term (called herein II) is the contribution of the surface energy change in the two caps due to solidification and can be estimated using the experimental bulk values of gold [21]. For elongated particles ($L \gg R$) this term is proportional to $L^{-1}$. Finally, the last term is due to the pressure change between the two phases.

Figure 4 reports the ratio $(T_s - T_0)/T_0$ obtained by MD calculations for all the studied cases as a function of the length of the particle $L$. In the same figure the term II of the rhs of (3) is plotted. From a comparison of the two curves it is clear that, within the intermediate range of particle sizes studied, term II alone captures quite well the behavior of the solidification point. However, in the limit of long particles, term II tends to zero, and (3) reduces to previous

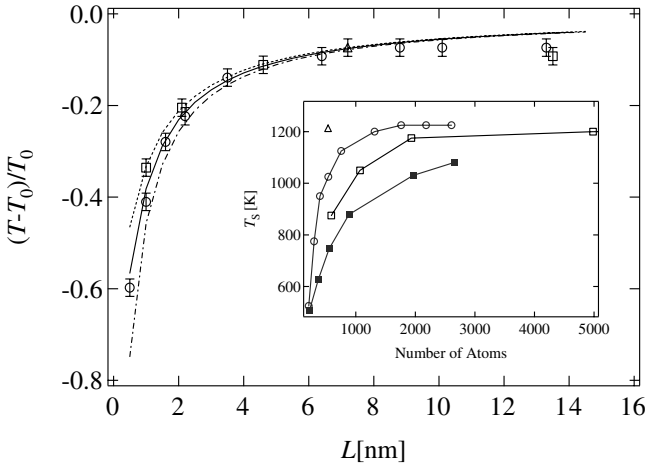


FIG. 4. Solidification curve as a function of particle length for all the studied cases. Markers, MD simulations: triangle, CNT (20, 0); circles, CNT (30, 0); squares, CNT (40, 0). Continuous lines, corresponding predictions of the second term (II) in the rhs of (3): dash-dotted line, CNT (20, 0); continuous line, CNT (30, 0); dashed line, CNT (40, 0). Inset: Solidification curve vs number of gold atoms in the particle. Closed squares: particles in vacuum; triangles: particles enclosed in a CNT (20, 0); circles: particles enclosed in a CNT (30, 0); squares: particles enclosed in a CNT (40, 0).

analytical findings for the crystallization of an infinite liquid medium inside a pore that predict a mere dependence on the radius [22] or the combined effect of radius and pressure [23]. In our case, the presence of the free caps allows the system to relax in the axial direction of the CNT. As a consequence, we expect the pressure difference $p_s - p_l$ to be small, in particular, for the case of short particles ($L < 10$ nm). Limiting our analysis to the short particle cases [and neglecting the third term in (3)], a fit to the MD data leads to $\Delta\gamma_{\text{C-Au}} \simeq 15$ mN/m for all CNT studied. We attribute this small change in $\Delta\gamma_{\text{C-Au}}$ to the collective nature of the cohesive gold-gold interactions in the particle, which renders the tendency to increase packing at the gold surface particularly strong. This leads to strongly close packed (100) and (111) surfaces both in the solid and in the liquid [24]. To quantify this tendency in our case, we compute the in-shell density for the different gold layers. We find that the outermost layer (the closest to the CNT) shows a lateral density of 15 atoms/Å$^2$ both for the solid and for the liquid phases across the solidification transition. Thus, the CNT interacts through a pairwise LJ potential with a close packed layer of gold in both phases. Averaged over the entire interface, the effect of this interaction should not change much across the phase transition. This fact, together with the observed layering effect in the liquid phase, is at the origin of the small value of $\Delta\gamma_{\text{C-Au}}$. As an example of the effect of the presence of the CNT, we note that in the case ($N_{\text{Au}} = 534$, $n = 20$) the particle has a length of 7.2 nm, with a solidification temperature of 1225 K, while a corresponding spherical cluster in vacuum solidifies at about 750 K.

For longer particles ($L > 10$ nm) the contribution of term II in (3) to the solidification temperature depression becomes of the same order as the other two terms in (3), and the MD results deviate from the continuous lines reaching a plateau. The particles enclosed in a CNT with $n = 40$ show a lower $T_s$ compared to the corresponding cases at $n = 30$. Moreover, in both cases, $T_s$ is lower than the value predicted by the sum of term II and term I in (3) with $\Delta\gamma_{\text{C-Au}} \simeq 15$ mN/m. This further reduction could be attributed to the role of the radial layering in the liquid phase. Particularly for long particles layering orders the structure, thus lowering the internal energy of the liquid phase. Even taking into account entropic effects, the free energy of the layered liquid phase is thus lower (at any temperature) than the one of the disordered liquid phase. This leads to a reduction of the solidification temperature.

To summarize, in this Letter the solidification and the structure of gold nanoparticles inside nanotubes have been studied using MD simulations. These particles have a higher solidification temperature than the corresponding isolated clusters, due to the presence of the CNT walls. The solid phase of the particle is characterized by analyzing the orientational order of each layer that consists of a 2D triangular structure, which is lost after the phase transition. On the contrary, the cylindrical layered structure persists in the liquid phase even at very high temperatures. Interestingly, within the range of tube radii considered, due to the influence of the free caps, the solidification temperature practically depends only on the length of the nanoparticle.

This work was supported by the Research Commission of ETHZ. We thank F. Ercolessi, E. Tosatti, and A. C. Levi for illuminating discussions.

*Corresponding author.

[1] W. Y. Choi, J. W. Kang, and H. J. Hwang, Phys. Rev. B **68**, 193405 (2003).
[2] J. W. Kang and H. J. Hwang, Nanotechnology **15**, 115 (2004).
[3] J. W. Kang and H. J. Hwang, J. Phys. Soc. Jpn. **73**, 738 (2004).
[4] O. Gulseren, F. Ercolessi, and E. Tosatti, Phys. Rev. Lett. **80**, 3775 (1998).
[5] Y. Kondo and K. Takayanagi, Science **289**, 606 (2000).
[6] B. L. Wang *et al.*, Phys. Rev. Lett. **86**, 2046 (2001).
[7] G. Bilalbegović, Phys. Rev. B **58**, 15 412 (1998).
[8] G. Bilalbegović, Solid State Commun. **115**, 73 (2000).
[9] Y. Guo *et al.*, J. Comput. Theor. Nanosci. **1**, 93 (2004).
[10] F. R. Hung *et al.*, Mol. Phys. **102**, 223 (2004).
[11] Z. W. Liu *et al.*, Phys. Rev. Lett. **93**, 095504 (2004).
[12] F. Ercolessi, M. Parrinello, and E. Tosatti, Philos. Mag. A **58**, 213 (1988).
[13] J. H. Walther *et al.*, J. Phys. Chem. B **105**, 9980 (2001).
[14] W. D. Luedtke and U. Landman, Phys. Rev. Lett. **82**, 3835 (1999); **83**, 1702 (1999).
[15] J. W. Kang *et al.*, J. Korean Phys. Soc. **43**, 534 (2003); H. J. Hwang, O. K. Kwon, and J. W. Kang, Solid State Commun. **129**, 687 (2004).
[16] L. J. Lewis *et al.*, Phys. Rev. B **61**, 16084 (2000).
[17] H. J. C. Berendsen *et al.*, J. Chem. Phys. **81**, 3684 (1984).
[18] O. Tomagnini *et al.*, Phys. Rev. Lett. **76**, 1118 (1996).
[19] P. J. Steinhardt, D. R. Nelson, and M. Ronchetti, Phys. Rev. B **28**, 784 (1983).
[20] S. Arcidiacono *et al.*, Int. J. Multiphase Flow **30**, 979 (2004); F. Ercolessi, W. Andreoni, and E. Tosatti, Phys. Rev. Lett. **66**, 911 (1991); L. J. Lewis, P. Jensen, and J. L. Barrat, Phys. Rev. B **56**, 2248 (1997).
[21] P. Buffat and J. P. Borel, Phys. Rev. A **13**, 2287 (1976).
[22] H. K. Christenson, J. Phys. Condens. Matter **13**, R95 (2001).
[23] R. Raj, Phys. Status Solidi A **166**, 529 (1998).
[24] M. Bernasconi and E. Tosatti, Surf. Sci. Rep. **17**, 363 (1993); F. Ercolessi, E. Tosatti, and M. Parrinello, Phys. Rev. Lett. **57**, 719 (1986).